Simulations of Steep Focused Waves Interaction with Fixed Cylinders using Fully Nonlinear Potential Flow and Navier-Stokes solvers in OpenFOAM

Zaibin Lin, Ling Qian, Wei Bai and Zhihua Ma
Centre for Mathematical Modelling and Flow Analysis, Department of Computing and Mathematics,
Manchester Metropolitan University, Manchester, M1 5GD, United Kingdom

ABSTRACT

As a commonly used foundation for coastal and offshore structures, cylindrical mono-pile foundations are theoretically suitable for intermediate water depth, where the waves may contains strong nonlinear components. The interaction between nonlinear waves and a cylindrical foundation is of importance in the engineering practice due to the the concern of survivability and stability of cylinder-support structures in extreme environmental conditions. In this paper, two different numerical models, Fully Nonlinear Potential Flow (FNPF) solver and Navier-Stokes (N-S) equations with Volume of Fluid (VoF) solver, are adopted to conduct comparative studies with a fixed cylinder in focused waves. Numerical results obtained by two different solvers are validated with released experimental measurements. Excellent agreements are presented, indicating both models are able to capture Wave-Structure Interaction, but with different applicability and efficiency.

KEY WORDS: Wave-structure interaction; Mono-pile foundation; Extreme wave conditions; Fully nonlinear potential flow; Navier-Stokes equations; OpenFOAM.

INTRODUCTION

Energy demand and global warning have driven the increasing investment and research activities for offshore renewable energy. The survivability of offshore renewable devices in extreme ocean environment remain challenging considering the effect of global and domestic climate change. In this circumstance, environmental conditions for offshore structures becomes even harsh, leading to unexpected loading on offshore structures and eventual damage. Therefore, the investigations on survivability and stability of offshore structures in the extreme environmental conditions are of importance and in a high demand.

As one of the primary concern, Wave-Structure Interaction (WSI) has gained growing attention in recent decades using various research approaches, such as numerical and experimental approaches. For numerical approaches, the Numerical Wave Tank (NWT) based on Naiver-Stokes equations and Volume of Fluid (NS-VoF) (Jacobsen et al., 2012; Higuera et al., 2013a,b; Martínez-Ferrer et al., 2018) has been increasingly populated in research and engineering communities (Lin et al., 2017; Chen et al., 2019), while as a efficient and accurate numerical model Fully Nonlinear Potential Flow (FNPF) model is able to solve the WSI problems under non-breaking waves (Bai and Taylor, 2007, 2009; Shao and Faltinsen, 2014; Lin et al., 2019; Ma et al., 2001a,b). Both numerical models have their own advantages in terms of Wave-Cylinder Iteration, such as high-fidelity for NS-VoF model and high-efficiency for FNPF model.

With the increasingly powerful computational capability, high-fidelity NS-VoF models have been widely applied to study Wave-Cylinder Interactions. Chen et al. (2014) systematically investigated the non-linear wave interactions with a cylindrical mono-pile foundation in regular and focused waves using OpenFOAM. They found that with sufficient mesh cells in a wave length, and adequate wave generation and absorption boundary conditions, NS-VoF model is able to provide accurate numerical results with acceptable speed. By using the numerical wave generation and absorption tools (waves2Foam) in OpenFOAM, Paulsen et al. (2014b) investigated the steep regular waves induced forcing on a fixed circular cylinder. It was concluded that the wave-induced 'ringing' phenomenon is more significant in deep water than that at intermediate water depth. Moreover, Paulsen et al. (2014a) proposed an efficient coupled FNPF-NS-VoF solver to investigate wave loads on a circular cylinder at intermediate water depth.

Apart from the time-consuming high-fidelity NS-VoF model, FNPF model is a comparatively efficient tool for WSI problems with excellent accuracy under non-breaking waves. Ma et al. (2001a,b) developed a 3-Dimensional Finite Element Method (FEM) FNPF solver to investigate the interactions between regular waves and a vertical fixed cylinder. Afterwards, Bai and Taylor (2007, 2009) proposed a time-domain FNFP model based on Boundary Element Method (BEM) to deal with the waves interactions with fixed and floating flared structures. For the novel spatial discretisations approach, Engsig-Karup et al. (2019) described A mixed Eulerian–Lagrangian Spectral Element Method (SEM) to investigate nonlinear wave interactions with fixed structures, and Bosi et al. (2019) developed a depth-integrated models using spectral/hp element method for the nonlinear WSI. Although Mehmood et al. (2015,

2016) have demonstrated the capability of OpenFOAM in fully solving the Laplace equation of velocity potential considering kinematic and dynamic free surface boundary conditions, they only presented the 2-Dimensional (2-D) wave generation and absorption of small steepness waves. Most recently, Lin et al. (2019) developed a 3-Dimensional (3-D) Finite Volume Method (FVM) based FNPF model in OpenFOAM to investigate WSI problems using OpenMPI parallel computing.

In order to examine the applicability of two NWTs for nonlinear wave interactions with a fixed cylinder for the comparative studies, the NS-VoF solver and recently developed inhouse FNPF solver in OpenFOAM (Lin et al., 2019) are adopted to reproduce the focused waves (Sriram et al., 2015) first, and then applied to study the interactions between focused waves and a fixed cylinder in comparison with released experimental measurements, although Yan et al. (2015) has demonstrated the different applicability of two aforementioned solvers. In this paper, the governing equations of two solvers are introduced thoroughly in section 2. The section 3 for wave generation and validations against experimental measurements is followed. In section 4, the nonlinear wave interactions with a fixed circular cylinder is presented with the comparison of the numerical results from two different NWTs. The conclusion of this study is summarised in section 5.

NUMERICAL MODELS

Two different numerical models are used for the investigations of WSI problems by comparing the numerical results with experimental measurements released for the comparative studies.

Navier-Stokes equations and Volume of Fluid

The governing equations for an incompressible and viscous flow are expressed as follows:

$$\nabla \cdot \boldsymbol{u} = 0 \tag{1}$$

$$\frac{\partial \rho \boldsymbol{u}}{\partial t} + \nabla \cdot (\rho \boldsymbol{u})\boldsymbol{u} - \nabla \cdot \mu \nabla \boldsymbol{u} = -\nabla p^* - (\boldsymbol{g} \cdot \boldsymbol{x})\nabla \rho \tag{2}$$

$$\frac{\partial \alpha}{\partial t} + \nabla \cdot \boldsymbol{u}\alpha + \nabla \cdot (\boldsymbol{u}_r \alpha(1-\alpha)) = 0 \tag{3}$$

where $\boldsymbol{u}$ is the velocity field, ρ is density of fluid, t is time, μ is dynamic viscosity of fluid, $p^* = p - \rho \boldsymbol{g} \cdot \boldsymbol{x}$ is the wave pressure, $\boldsymbol{g}$ is gravitational acceleration, $\boldsymbol{x} = (x, y, z)$ is the Cartesian coordinate system, α is the volume fraction, and $\boldsymbol{u_r}$ is compressive velocity field proposed in Berberović et al. (2009), maintaining the sharp water-air interface. By introducing the wave generation boundary condition, the target second-order focused waves are generated in the NWT using NweWave formulation up to second-order harmonics. Readers are referred to Hu et al. 2016 and Chen et al. 2019 for more details. The outgoing waves are absorbed by the active wave absorption boundary conditions in Higuera et al. (2013a,b).

Fully Nonlinear Potential Flow model

On the basis of the assumption of FNPF model that the fluid is irrorational and inviscid, the governing equations is described as follow:

$$\nabla^2 \phi = 0 \tag{4}$$

where ϕ is the velocity potential. Introducing both the kinematic (Eqn. 5) and dynamic (Eqn. 6) free surface boundary conditions in a mixed-Eulerian-Lagrangian form to Eqn. 4 provides the solutions for wave propagation and transformation.

$$\frac{\partial \eta}{\partial t} = \frac{\partial \phi}{\partial y} - \frac{\partial \phi}{\partial x}\frac{\partial \eta}{\partial x} - \frac{\partial \phi}{\partial z}\frac{\partial \eta}{\partial z} = \frac{\boldsymbol{U_\eta} \cdot \boldsymbol{n}}{n_y} \tag{5}$$

$$\frac{\delta \phi}{\delta t} = -\boldsymbol{g}\eta - \frac{1}{2}\nabla\phi \cdot \nabla\phi + \frac{\partial \eta}{\partial t}\frac{\partial \phi}{\partial y} \tag{6}$$

where η is free surface elevation, $\boldsymbol{U_\eta}$ is the fluid particle velocity at free surface, $\boldsymbol{n}$ is the unit normal vector on the free surface pointing outwards the numerical domain, and n_y is the vertical component of $\boldsymbol{n}$. Readers are referred to Lin et al. (2019) for more details of this FNPF model in OpenFOAM.

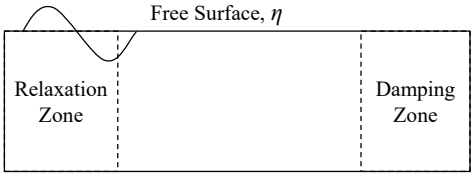

Fig. 1 Sketch of FNPF numerical wave tank

To generate progressive waves and absorb reflected waves, a relaxation zone is positioned at the left side of NWT shown in Fig. 1.Inside this zone a relaxation function is specified as follows (Bingham and Zhang, 2007):

$$\alpha_R(\chi_R) = 1 - \frac{\exp(\chi_R^{3.5}) - 1}{\exp(1) - 1} \tag{7}$$

$$\eta = \alpha_R \eta_{\text{computed}} + (1 - \alpha_R)\eta_{\text{target}} \tag{8}$$

$$\phi = \alpha_R \phi_{\text{computed}} + (1 - \alpha_R)\phi_{\text{target}} \tag{9}$$

where χ_R is the function that equals to 0 at the inlet and equals to 1 at the end of relaxation zone linking to the non-relaxation zone. Then this relaxation function is applied generate waves and absorb reflected waves by weighting computed and target free surface elevation and velocity potential at free surface. While inside the damping zone, two additional damping terms are added to kinematic and dynamic free surface boundary conditions, respectively:

$$\frac{\partial \eta}{\partial t} = \frac{\boldsymbol{U_\eta} \cdot \boldsymbol{n}}{n_y} - \nu_\eta(x)(\eta - \eta_s) \tag{10}$$

$$\frac{\delta \phi}{\delta t} = -\boldsymbol{g}\eta - \frac{1}{2}\nabla\phi \cdot \nabla\phi + \frac{\partial \eta}{\partial t}\frac{\partial \phi}{\partial y} - \nu_\eta(x)\phi \tag{11}$$

$$\nu_\eta(x) = \begin{cases} \alpha_{\text{damping}}\omega(\dfrac{x - x_0}{\beta_{\text{damping}}\lambda})^2, & x \geq x_0 \\ 0, & x < x_0 \end{cases} \tag{12}$$

where x_0 is the location connecting the non-damping zone; α_{damping} and β_{damping} are the damping coefficients related to sponge layer strength and legnth, respectively; η_s is the free surface elevation at rest; λ is wave length, and ω is wave frequency. The second-order NewWave formulations (Hu et al., 2016) are also adopted in FNPF model to generate focused waves.

NUMERICAL SETUPS

Before applying both NS-VoF and FNPF models into investigating the WSI problems, the mesh sensitivity study are performed first in order to obtain mesh convergence for further applications. For NS-VoF model, Chen et al. (2014) recommended 70 cells Per Wave Length (PWL), which is sufficient for maintaining the numerical results convergent.

Table 1 Mesh setups for mesh sensitivity study of FNPF model

Mesh ID	Mesh setup (x, y, z)	Cells PWL
1	60×10×1	15
2	80×10×1	20
3	100×10×1	25

Nevertheless, the cell PWL for FNPF model is much less than that of NS-VoF model. Therefore, the mesh sensivitivity study is conducted in this section for FNPF model. The total mesh numbers and cell numbers PWL are listed in Table 1.

In Fig. 2, the free surface elevation at the the centre of NWT are presented with 3 different mesh setups, as well as analytical solution of second-order Stokes waves. It is clearly denoted that the mesh setup with less cells PWL (15 cells) is not able to maintain the stability of progressive wave profile. However, inceasing the cell numbers PWL to 20 significantly improve the stability of progressive wave profile in the NWT. Only a slight difference can be noticed between the cases of Mesh ID 2 (20 cells PWL) and Mesh ID 3 (25 cells PWL). The further applications of the FNPF model mesh setup follows the conclusion that 20 cells PWL at least is adopted for FNPF NWT domain.

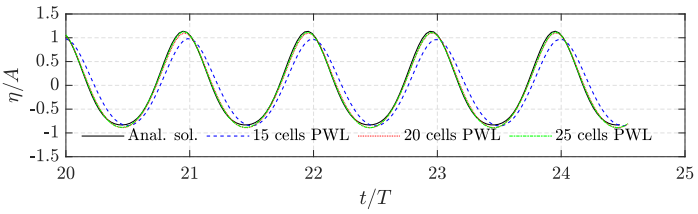

Fig. 2 Mesh convergence study of FNPF model

FOCUSED WAVE GENERATION

Due to the limited computational resources for full representation of wave flume in the laboratory, the focused location is modified to 12m, instead of 23m in the laboratory, away from wave maker to minimise computational efforts. Therefore, the total length of NWT for both numerical models is 24m, in which the centre of a fixed cylinder is located at 13.88m away from wave maker. The mesh for NS-VoF model is uniformly distributed within the zone of 0m $< x <$ 15m in x direction, and the mesh inside the zone of 15m $< x <$ 24m is horizontally stretched, which maintains the denser mesh at 15m and coarser mesh at 24m. In the y direction, the mesh is refined within $-0.25\text{m} < y < 0.15\text{m}$ in order to cover all pressure gauges. A similar horizontal mesh layout is used for FNPF model, while with less amount of mesh number, while in vertical direction the mesh is stretched from the bottom to water surface with mesh refinement near free surface as there is no additional mesh required to model air flow in FNPF model. These two different mesh layouts are presented in Fig. 3 for clarity. Total amounts of two mesh layouts are approximately 11.4 million and 71.4 thousand, respectively.

As a shorter NWT is set up for comparative study, the Wave Gauge 1 (WG1), recommended in the comparative study call for wave generation validation, is not adopted here to verify the quality of target numerical focused waves. Instead, the remaining WGs in the laboratory are adopted to validate numerical focused waves. The locations of these wave gauges are tabulated in Table 2, and the locations in other

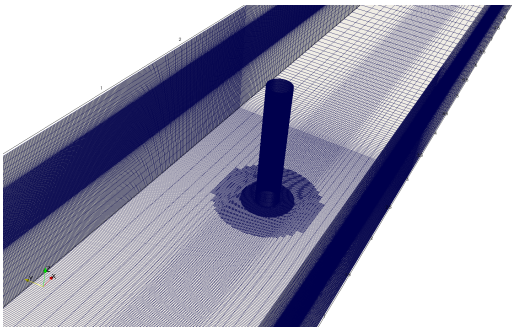

(a) Mesh layout for NS-VoF model

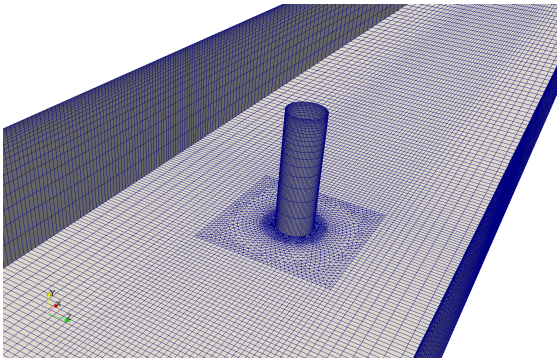

(b) Mesh layout for FNPF model

Fig. 3 Mesh layouts for two different NWTs

Table 2 Distance of Wave gauges from wave maker (m)

WGs ID	WG2	WG3	WG4	WG5	WG6	WG7
Lab.	13.928	14.178	14.428	24.31	24.88	25.585
NWT	2.928	3.178	3.428	13.31	13.88	14.585

Table 3 Wave parameters for focused waves

Wave ID	$f_1(Hz)$	f_N(Hz)	N	$t_f(s)$	x_f(m)	G_a
W1	0.34	1.02	32	29	12	0.001
W2	0.34	1.02	32	29	12	0.003

directions remains the identical as experiments.Wave parameters are listed in Table 3. The NS-VoF model covered the WSI simulations of two cases, while FNPF model only conducted the WSI simulation of case W1 and wave only for case W2. As significant wave breaking occurs for case W2 in both numerical and experimental results, it is not the applicability of FNPF model.

With the presence of a fixed cylinder in wave tank, numerical results of two different models are shown in Figs. 4 and 5, together with experimental measurements. Good agreements between numerical and experimental results demonstrate that both the NS-VoF model and FNPF model are able to reproduce the focused waves based on second-order wave maker theory, although slight phase differences are noticed for WG3 and WG4 in Fig. 4. In addition to case W1, the numerical results of case W2 using NS-VoF model and FNPF model are indicated in Figs. 6 and 7, together with experimental data. Overall good agreements are obtained for this large steepness focused waves, while slight discrepancy of wave phase is shown at WG3 and WG4 in Fig. 6 as the same for case W1. Moreover, it is clearly denoted from both numerical and experimental results at WGs

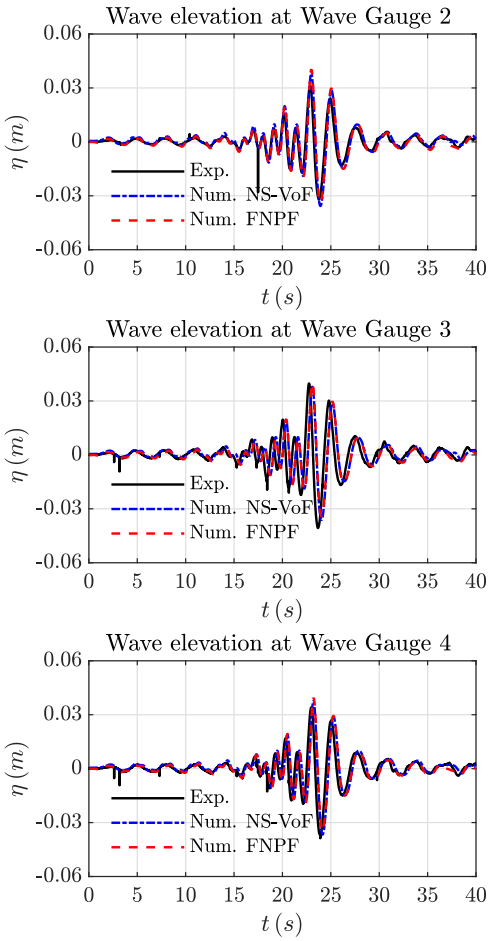

Fig. 4 Comparisons of numerical results using NS-VoF model and FNPF model with experimental measurements: WG2-WG4 of case W1

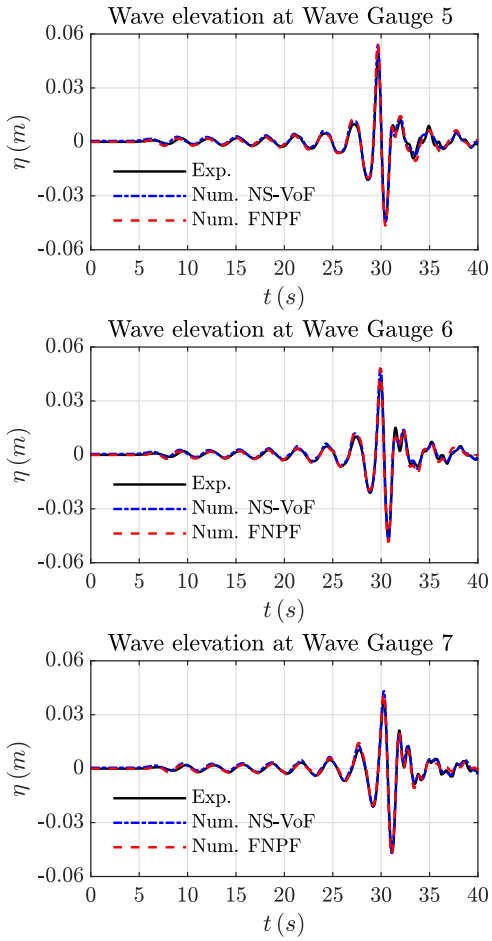

Fig. 5 Comparisons of numerical results using NS-VoF model and FNPF model with experimental measurements: WG5-WG7 of case W1

5-7 that after focal location x=12m the wave breaking occurs and evident fluctuations of free surface are certainly recorded by WGs 5-7. Without energy dissipation from wave-breaking phenomenon, free surface elevations η at WGs 5-7 using FNPF model show larger magnitude compared to the results from NS-VoF model that is able to accurately predict wave-breaking and associated energy dissipation. This process of spilling wave breaking is shown in Fig. 8.

WAVE-CYLINDER INTERACTION

When a cylinder is positioned in the wave tank, incident focused waves impose oscillatory wave pressure on the structure surface. In this section, the numerical wave pressure at the locations listed in Table 4 are compared with released experimental measurements in Figs. 9 and 10. Excellent agreements with experimental measurements can be found from the numerical results based on NS-VoF model and FNPF model, demonstrating that two different models are fully capable of capturing the WSI problem under non-breaking waves (case W1) and that FNPF model takes the advantage of efficiency compared to NS-VoF solver under this circumstance of non-breaking waves. For the efficiency, FNPF model only took less than 10 hours with 16 cores to complete the simulation, while NS-VoF model required more than 32 hours with 96 cores to complete simulation. However, FNFP model is not able to predict the WSI process after wave-breaking, which is the advantage of NS-VoF model. Therefore under breaking waves (case W2), only the numerical results using NS-VoF model are compared with experimental data in Figs. 11 and 12, where excellent agreements are obtained even after wave breaking. It can be clearly seen from Fig. 13 that after focused time t_f significant wave breaking occurs in the vicinity of a fixed cylinder, leading to the evident pressure fluctuation in Figs. 11 and 12 when t = 40-45s. This breaking wave case W2 took approximately 101 hours with 96 cores. By taking these advantages, it is highly recommended to integrate both NS-VoF model and FNPF model in a two way manner with efficient parallel computing.

Table 4 Pressure Gauges (PGs) locations around cylinder (m)

PGs ID	PG1	PG2	PG3	PG4	PG5	PG6	PG7	PG8
Location	−0.285	−0.185	−0.085	0.015	0.115	−0.085	−0.085	−0.085
Angle(°)	0	0	0	0	0	20	90	180

Note: vertical location of Pressure Gauges (PGs) is relative to the still water level and 0° indicates the direction towards wave maker.

CONCLUSIONS AND DISCUSSION

This paper presents the comparative study of two different models, namely NS-VoF model and FNPF model in OpenFOAM. Excellent

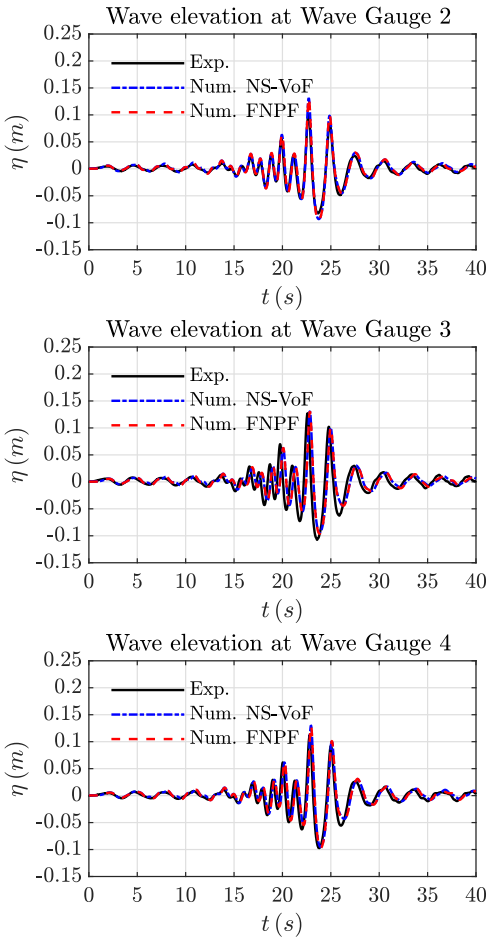

Fig. 6 Comparisons of numerical results using NS-VoF model and FNPF model with experimental measurements: WG2-WG4 of case W2

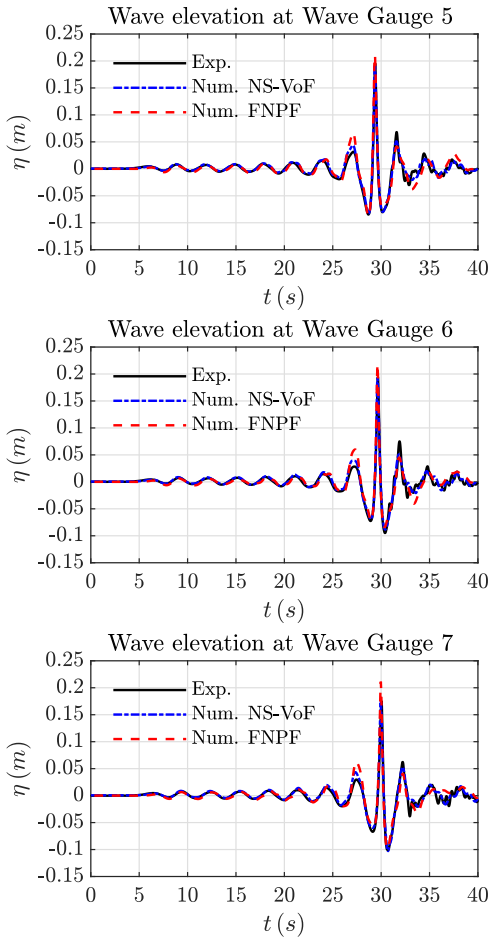

Fig. 7 Comparisons of numerical results using NS-VoF model and FNPF model with experimental measurements: WG5-WG7 of case W2

agreements have been demonstrated by validating numerical results against released experimental measurements, even with breaking waves. The pros and cons of both NS-VoF model and FNPF model are explicitly demonstrated in terms of their efficiency and applicability. FNPF model provides the efficiency under non-breaking waves, while NS-VoF model is capable of capturing breaking wave interactions with structure in detail. Therefore, the future work is to integrate the FNFP model and NS-VoF model in OpenFOAM in a two-way manner, allowing highly efficient and massively parallel computing through OpenMPI.

ACKNOWLEDGMENTS

This work was partially funded by the Engineering and Physical Sciences Research Council (EPSRC, UK) projects: A Zonal CFD Approach for Fully Nonlinear Simulations of Two Vessels in Launch and Recovery Operations (EP/N008839/1), Extreme Loading on FOWT under Complex Environmental Conditions (EP/T004150/1), and A CCP on Wave Structure Interaction: CCP-WSI (EP/M022382/1). The first author would also like to acknowledge the financial support from the Manchester Metropolitan University through sponsoring a Research Associate position.

REFERENCES

Bai, W., and Taylor, R. E. (2007). Numerical simulation of fully nonlinear regular and focused wave diffraction around a vertical cylinder using domain decomposition. *Applied Ocean Research*, *29*(1-2), 55–71.

Bai, W., and Taylor, R. E. (2009). Fully nonlinear simulation of wave interaction with fixed and floating flared structures. *Ocean engineering*, *36*(3-4), 223–236.

Berberović, E., van Hinsberg, N. P., Jakirlić, S., Roisman, I. V., and Tropea, C. (2009). Drop impact onto a liquid layer of finite thickness: Dynamics of the cavity evolution. *Physical Review E*, *79*(3), 036306.

Bingham, H. B., and Zhang, H. (2007). On the accuracy of finite-difference solutions for nonlinear water waves. *Journal of Engineering Mathematics*, *58*(1-4), 211–228.

Bosi, U., Engsig-Karup, A. P., Eskilsson, C., and Ricchiuto, M. (2019). A spectral/hp element depth-integrated model for nonlinear wave–body interaction. *Computer Methods in Applied Mechanics and Engineering*, *348*, 222–249.

Chen, H., Qian, L., Bai, W., Ma, Z., Lin, Z., and Xue, M.-A. (2019). Oblique focused wave group generation and interaction with a fixed fpso-shaped body: 3d cfd simulations and comparison with experiments. *Ocean Engineering*, *192*, 106524.

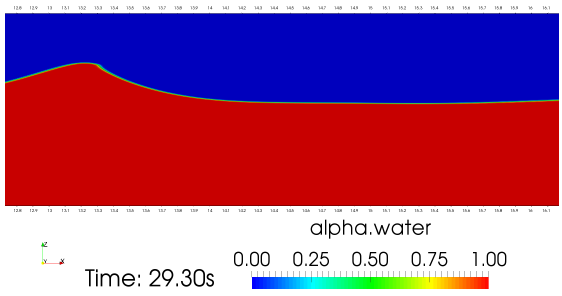

(a) t = 29.30s

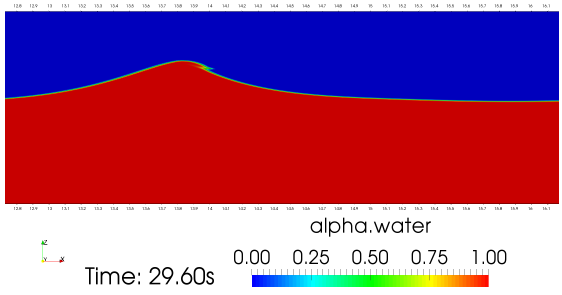

(b) t = 29.60s

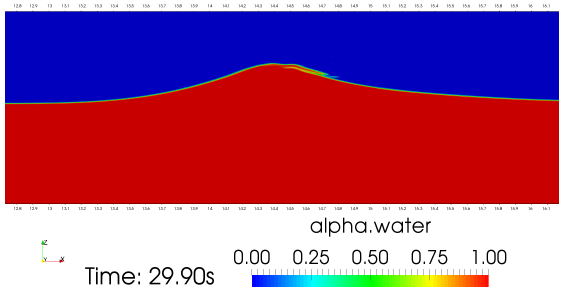

(c) t = 29.90s

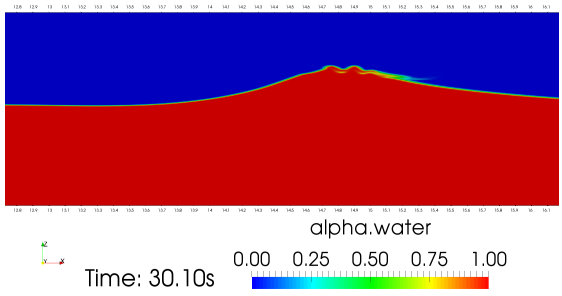

(d) t = 30.10s

Fig. 8 Snapshots of Wave breaking for case W2 at different moments using NS-VoF model

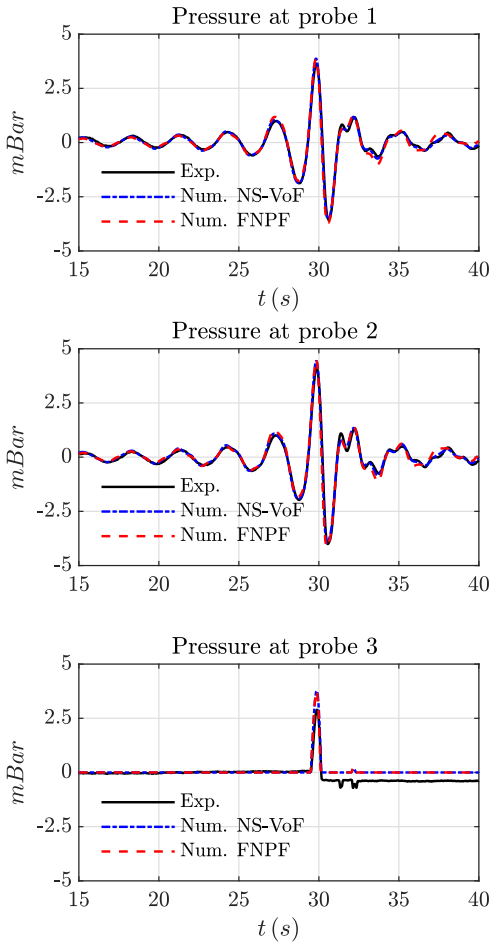

Fig. 9 Comparisons of numerical results using NS-VoF model and FNPF model with experimental measurements: PG1-PG3 of case W1

Chen, L., Zang, J., Hillis, A. J., Morgan, G. C., and Plummer, A. R. (2014). Numerical investigation of wave-structure interaction using OpenFOAM. *Ocean Engineering*, *88*, 91–109.

Engsig-Karup, A. P., Monteserin, C., and Eskilsson, C. (2019). A mixed eulerian–lagrangian spectral element method for nonlinear wave interaction with fixed structures. *Water Waves*, *1*(2), 315–342.

Higuera, P., Lara, J. L., and Losada, I. J. (2013a). Realistic wave generation and active wave absorption for Navier-Stokes models: Application to OpenFOAM®. *Coastal Engineering*, *71*, 102–118.

Higuera, P., Lara, J. L., and Losada, I. J. (2013b). Simulating coastal engineering processes with OpenFOAM®. *Coastal Engineering*, *71*, 119–134.

Hu, Z. Z., Greaves, D., and Raby, A. (2016). Numerical wave tank study of extreme waves and wave-structure interaction using OpenFoam®. *Ocean Engineering*, *126*, 329–342.

Jacobsen, N. G., Fuhrman, D. R., and Fredsøe, J. (2012). A wave generation toolbox for the open-source cfd library: Openfoam®. *International Journal for numerical methods in fluids*, *70*(9), 1073–1088.

Lin, Z., Pokrajac, D., Guo, Y., Jeng, D.-S., Tang, T., Rey, N., … Zhang, J. (2017). Investigation of nonlinear wave-induced seabed response around mono-pile foundation. *Coastal Engineering*, *121*, 197–211.

Lin, Z., Qian, L., Bai, W., Ma, Z., Chen, H., and Zhou, J.-G. (2019). Development of 3-dimensional fully nonlinear potential flow planar wave tank in framework of openfoam. In *ASME 2019 38th International Conference on Ocean, Offshore and Arctic Engineering*.

Ma, Q., Wu, G., and Eatock Taylor, R. (2001a). Finite element simulation of fully non-linear interaction between vertical cylinders and steep waves. part 1: methodology and numerical procedure. *International Journal for Numerical Methods in Fluids*, *36*(3), 265–285.

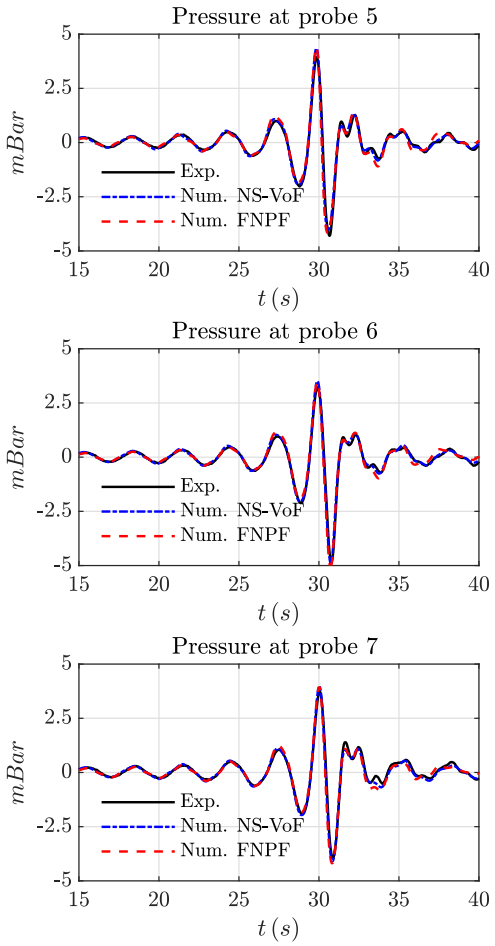

Fig. 10 Comparisons of numerical results using NS-VoF model and FNPF model with experimental measurements: PG5-PG7 of case W1

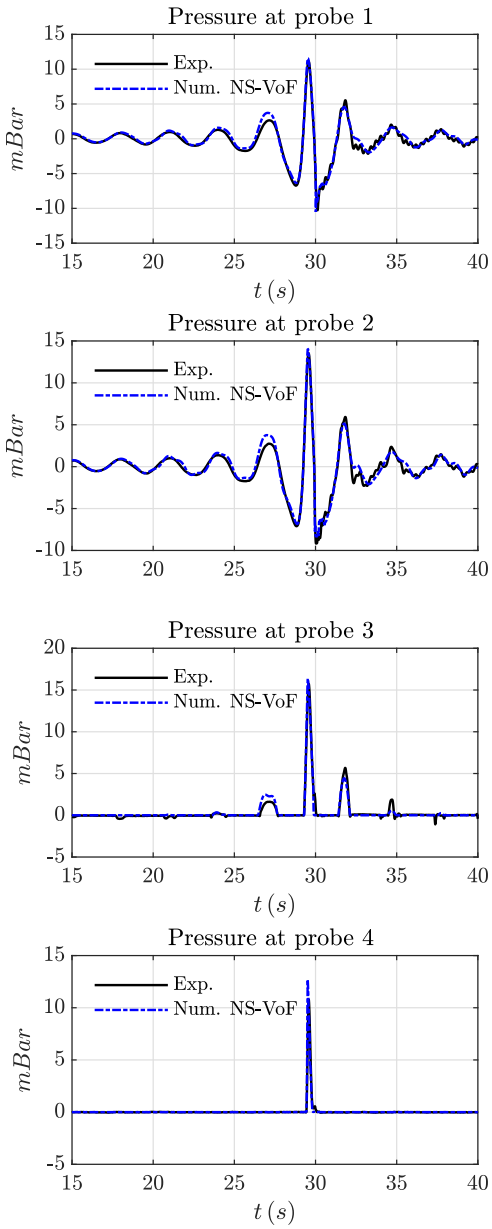

Fig. 11 Comparisons of numerical results using NS-VoF model and FNPF model with experimental measurements: PG1-PG4 of case W2

Ma, Q., Wu, G., and Eatock Taylor, R. (2001b). Finite element simulations of fully non-linear interaction between vertical cylinders and steep waves. part 2: numerical results and validation. *International Journal for Numerical Methods in Fluids*, *36*(3), 287–308.

Martínez-Ferrer, P. J., Qian, L., Ma, Z., Causon, D. M., and Mingham, C. G. (2018). Improved numerical wave generation for modelling ocean and coastal engineering problems. *Ocean Engineering*, *152*, 257–272.

Mehmood, A., Graham, D. I., Langfeld, K., Greaves, D. M., et al. (2015). Openfoam finite volume method implementation of a fully nonlinear potential flow model for simulating wave-structure interactions. In *The Twenty-fifth International Ocean and Polar Engineering Conference.*

Mehmood, A., Graham, D. I., Langfeld, K., Greaves, D. M., et al. (2016). Numerical simulation of nonlinear water waves based on fully nonlinear potential flow theory in openfoam®-extend. In *The 26th International Ocean and Polar Engineering Conference.*

Paulsen, B. T., Bredmose, H., and Bingham, H. B. (2014a). An efficient domain decomposition strategy for wave loads on surface piercing circular cylinders. *Coastal Engineering*, *86*, 57–76.

Paulsen, B. T., Bredmose, H., Bingham, H. B., and Jacobsen, N. G. (2014b). Forcing of a bottom-mounted circular cylinder by steep regular water waves at finite depth. *Journal of fluid mechanics*, *755*, 1–34.

Shao, Y.-L., and Faltinsen, O. M. (2014). A harmonic polynomial cell (hpc) method for 3d laplace equation with application in marine hydrodynamics. *Journal of Computational Physics*, *274*, 312–332.

Sriram, V., Schlurmann, T., and Schimmels, S. (2015). Focused wave evolution using linear and second order wavemaker theory. *Applied Ocean Research*, *53*, 279–296.

Yan, S., Ma, Q., Sriram, V., Qian, L., Ferrer, P., Schlurmann, T., et al. (2015). Numerical and experimental studies of moving cylinder in uni-directional focusing waves. In *The Twenty-fifth International Ocean and Polar Engineering Conference.*

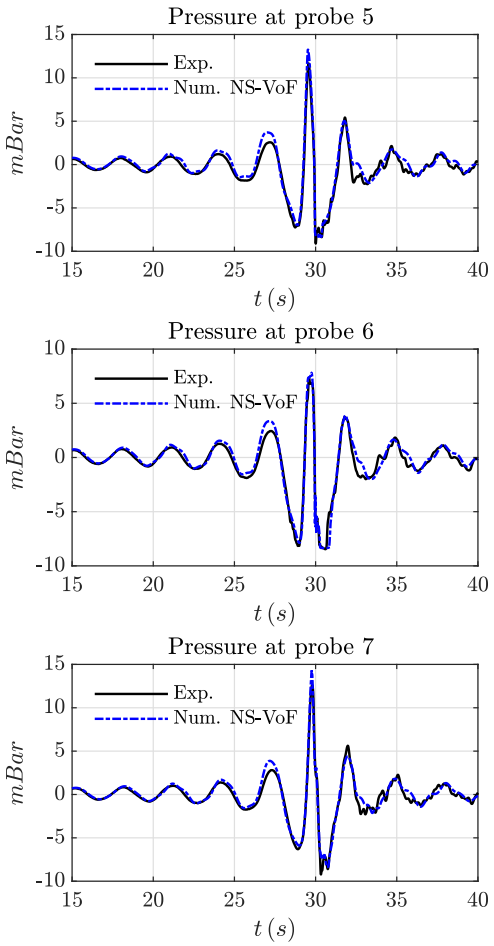

Fig. 12 Comparisons of numerical results using NS-VoF model and FNPF model with experimental measurements: PG5-PG7 of case W1

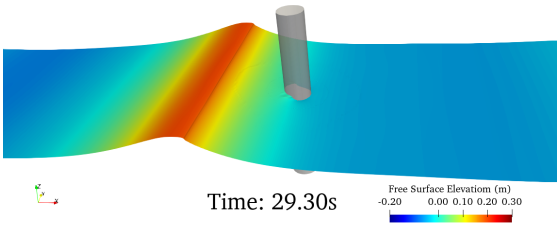

(a) t = 29.30s

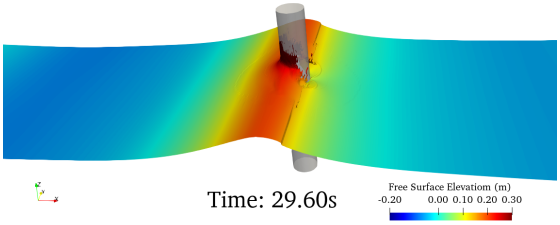

(b) t = 29.60s

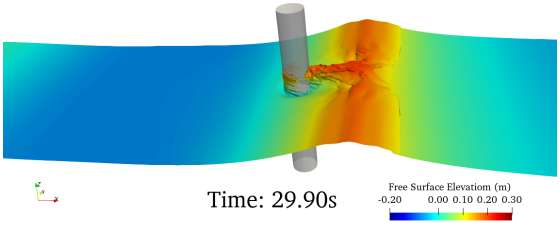

(c) t = 29.90s

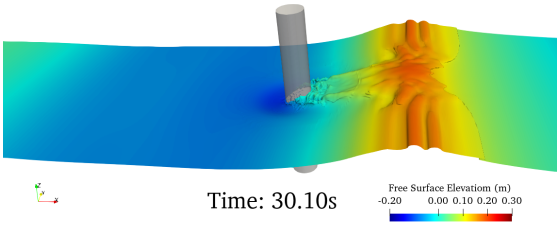

(d) t = 30.10s

Fig. 13 Snapshots of Wave breaking for case W2 around cylinder at different moments using NS-VoF model